IL NUOVO CIMENTO Vol. 34 C, N. 4 Luglio-Agosto 2011
DOI 10.1393/ncc/i2011-10970-2

Colloquia: Channeling 2010

On the ratio of the relativistic electron PXR in Bragg and forward direction within Bragg scattering geometry

S. Blazhevich([1]) and A. Noskov([2])

([1]) *Belgorod State University - Belgorod, Russia*
([2]) *Belgorod University of Consumer's Cooperation - Belgorod, Russia*

(ricevuto il 22 Dicembre 2010; pubblicato online il 21 Settembre 2011)

Summary. — In the present work, the parametric X-radiation (PXR) and the parametric radiation at a small angle relative to the velocity of a relativistic electron (FPXR) crossing a single crystal plate in Bragg scattering geometry are investigated within the framework of the dynamic X-ray diffraction theory. The expressions for spectral-angular density of the named radiations are derived in the general case of asymmetric reflection. The ratio of the contributions of these radiation mechanisms as a function of reflection asymmetry is considered in this work.

PACS 41.60.-m – Radiation by moving charges.
PACS 41.75.Ht – Relativistic electron and positron beams.
PACS 42.25.Fx – Diffraction and scattering.

1. – Introduction

When a fast charged particle crosses a single crystal its Coulomb field pseudo photons scatter on the system of parallel atomic planes generating parametric X-radiation (PXR) [1-3]. The theory of PXR of relativistic particle in a crystal forecasts the radiation not only in Bragg scattering direction, but also in the direction of radiating particle velocity (FPXR) [4-6], which represents the appearance of dynamical diffraction in PXR. It is known that some attempts of the FPXR experimental research were made [7-11], but the first report about its experimental discovery has appeared recently in ref. [11], where the FPXR was registered in Laue scattering geometry. In the experiment [11] the relativistic electron X-radiation was registered in the condition of FPXR generation, nevertheless the sought-for peak became weakly apparent on the background of the radiation generated by scattered electrons in the structural material of the experimental setup. Thus the theoretical investigations of FPXR properties and the optimization of viewing conditions for experimental observation of this dynamical effect remain topical up to date.

The detailed theoretical description of dynamical effect of FPXR and its accompanying transition radiation (TR), as a background, was made for the case of symmetrical

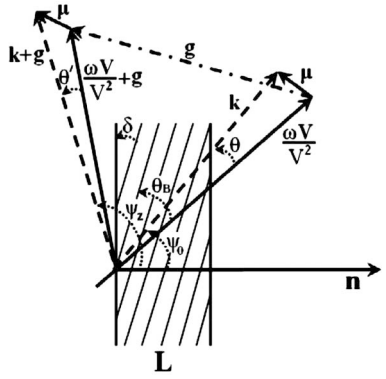

Fig. 1. – Radiation process geometry.

reflection in the works [12-15]. Under condition of asymmetrical reflection of the relativistic electron Coulomb field the PXR, TR and DTR were theoretically investigated in refs. [16-18] and FPXR in Bragg geometry in ref. [19]. The above-mentioned works showed that the spectral-angular density of these radiation mechanisms depends essentially on the reflection asymmetry and revealed the effects associated with it. The ratio of PXR and FPXR yield in Laue scattering geometry was considered in [20], where it was shown that the change of the reflection asymmetry cardinally changes the ratio.

In the present work the analytical expressions for spectral-angular density of FPXR are derived in the framework of two-wave approximation of dynamic diffraction theory [21] in general case of asymmetrical field reflection. Based on the obtained expressions the ratio of PXR and FPXR yields is investigated as a function of reflection asymmetry in Bragg scattering geometry.

2. – Dynamical expressions for electric fields in crystal target

Let us consider the radiation of a fast charged particle crossing a single crystal plate with a constant velocity $\mathbf{V}$ (see in fig. 1). We will use the same table of symbols as in the work [17].

While solving the problem, let us consider an equation for a Fourier image of an electromagnetic field

$$\mathbf{E}(\mathbf{k},\omega) = \int \mathrm{d}t\mathrm{d}^3 r \mathbf{E}(\mathbf{r},t)\exp[i\omega t - i\mathbf{kr}]. \tag{1}$$

Since the field of a relativistic particle could, to a good accuracy, be taken as being transverse, the incident $\mathbf{E}_0(\mathbf{k},\omega)$ and diffracted $\mathbf{E}_\mathbf{g}(\mathbf{k},\omega)$ electromagnetic waves are determined by two amplitudes with different values of transverse polarization:

$$\begin{aligned}\mathbf{E}_0(\mathbf{k},\omega) &= E_0^{(1)}(\mathbf{k},\omega)\mathbf{e}_0^{(1)} + E_0^{(2)}(\mathbf{k},\omega)\mathbf{e}_0^{(2)},\\ \mathbf{E}_\mathbf{g}(\mathbf{k},\omega) &= E_\mathbf{g}^{(1)}(\mathbf{k},\omega)\mathbf{e}_1^{(1)} + E_\mathbf{g}^{(2)}(\mathbf{k},\omega)\mathbf{e}_1^{(2)},\end{aligned} \tag{2}$$

where the unit vectors of polarization $\mathbf{e}_0^{(1)}$ and $\mathbf{e}_0^{(2)}$ are perpendicular to vector $\mathbf{k}$, and

vectors $\mathbf{e}_1^{(1)}$ and $\mathbf{e}_1^{(2)}$ are perpendicular to vector $\mathbf{k}_g = \mathbf{k} + \mathbf{g}$. Vectors $\mathbf{e}_0^{(2)}$, $\mathbf{e}_1^{(2)}$ are situated on the plane of vectors $\mathbf{k}$ and $\mathbf{k}_g$ (π-polarization) and $\mathbf{e}_0^{(1)}$, $\mathbf{e}_1^{(1)}$ are perpendicular to this plane (σ-polarization); $\mathbf{g}$ is vector of the reciprocal lattice, defining a set of reflecting atomic planes. The system of equation for the Fourier transform images of electromagnetic field in two-wave approximation of dynamic theory of diffraction has the following view [22]:

$$(3)\qquad \begin{cases} (\omega^2(1+\chi_0) - k^2)E_0^{(s)} + \omega^2\chi_{-\mathbf{g}}C^{(s,\tau)}E_{\mathbf{g}}^{(s)} = 8\pi^2 ie\omega\theta V P^{(s)}\delta(\omega - \mathbf{kV}), \\ \omega^2\chi_{\mathbf{g}}C^{(s,\tau)}E_0^{(s)} + (\omega^2(1+\chi_0) - k_{\mathbf{g}}^2)E_{\mathbf{g}}^{(s)} = 0, \end{cases}$$

where $\chi_0 = \chi_0' + i\chi_0''$ is the average dielectric susceptibility, $\chi_{\mathbf{g}}$, $\chi_{-\mathbf{g}}$ are the coefficients of the Fourier expansion of the dielectric susceptibility of a crystal over the reciprocal lattice vectors $\mathbf{g}$:

$$(4)\qquad \chi(\omega, \mathbf{r}) = \sum_{\mathbf{g}} \chi_{\mathbf{g}}(\omega)e^{i\mathbf{gr}} = \sum_{\mathbf{g}} \left(\chi_{\mathbf{g}}'(\omega) + i\chi_{\mathbf{g}}''(\omega)\right) e^{i\mathbf{gr}}.$$

The values $\tilde{N}^{(s,\tau)}$ and $P^{(s)}$ are defined in the system (3) as

$$(5)\qquad C^{(s,\tau)} = \boldsymbol{e}_0^{(s)}\boldsymbol{e}_1^{(s)} = (-1)^\tau C^{(s)}, \qquad \tilde{N}^{(1)} = 1, \qquad \tilde{N}^{(2)} = |\cos 2\theta_B|,$$

$$P^{(s)} = \boldsymbol{e}_0^{(s)}(\boldsymbol{\mu}/\mu), \qquad P^{(1)} = \sin\varphi, \qquad P^{(2)} = \cos\varphi,$$

$\boldsymbol{\mu} = \mathbf{k} - \omega\mathbf{V}/V^2$ is the virtual photon momentum vector component perpendicular to the particle velocity vector $\mathbf{V}$ ($\mu = \omega\theta/V$, where $\theta \ll 1$ is the angle between $\mathbf{k}$ and $\mathbf{V}$), θ_B is the angle between electron velocity and a set of atomic planes in the crystal (Bragg angle), φ is the azimuth angle, counted off from the plane formed by vectors $\mathbf{V}$ and $\mathbf{g}$, the value of the reciprocal lattice vector is shown by the expression $g = 2\omega_B \sin\theta_B/V$, ω_B is Bragg's frequency. The angle between vector $\frac{\omega\mathbf{V}}{V^2} + \mathbf{g}$ and diffracted wave vector $k_{\mathbf{g}}$ is defined as θ'. The equation system (3) under $s = 1$ describes the fields of σ-polarization, and under $s = 2$ the fields of π-polarization. When $2\theta_B < \frac{\pi}{2}$, then $\tau = 2$, otherwise $\tau = 1$.

Let us solve the dispersion equation for X-waves in crystal following from system (3):

$$(6)\qquad (\omega^2(1+\chi_0) - k^2)(\omega^2(1+\chi_0) - k_{\mathbf{g}}^2) - \omega^4\chi_{-\mathbf{g}}\chi_{\mathbf{g}}C^{(s)^2} = 0,$$

using standard methods of dynamic theory [21]

$$(7)\qquad k = \omega\sqrt{1+\chi_0} + \lambda_0, \qquad k_{\mathbf{g}} = \omega\sqrt{1+\chi_0} + \lambda_{\mathbf{g}},$$

$$(8)\qquad \lambda_0^{(1,2)} = \omega\frac{\gamma_0}{4\gamma_{\mathbf{g}}}\left(-\beta \pm \sqrt{\beta^2 + 4\chi_{\mathbf{g}}\chi_{-\mathbf{g}}C^{(s)^2}\frac{\gamma_{\mathbf{g}}}{\gamma_0}}\right),$$

$$\lambda_{\mathbf{g}}^{(1,2)} = \frac{\omega}{4}\left(\beta \pm \sqrt{\beta^2 + 4\chi_{\mathbf{g}}\chi_{-\mathbf{g}}C^{(s)^2}\frac{\gamma_{\mathbf{g}}}{\gamma_0}}\right).$$

where $\beta = \alpha - \chi_0(1 - \frac{\gamma_{\mathbf{g}}}{\gamma_0})$, $\alpha = \frac{1}{\omega^2}(k_{\mathbf{g}}^2 - k^2)$, $\gamma_0 = \cos\psi_0$, $\gamma_{\mathbf{g}} = \cos\psi_{\mathbf{g}}$, ψ_0 is the angle

between the incident wave vector $\boldsymbol{k}$ and the vector normal to the plate surface $\mathbf{n}$, ψ_g is the angle between wave vector $\mathbf{k_g}$ and the vector $\mathbf{n}$ (see fig. 1).

As $|\lambda_0| \ll \omega$ and $|\lambda_\mathbf{g}| \ll \omega$, we can show that $\theta \approx \theta'$ (see in fig. 1), and hereinafter will use θ in all the occasions.

The solution of the combined equations (3) gives us the relativistic particle field in the vacuum in front of the crystal as

$$E_0^{(s)\mathrm{vac\,I}} = \frac{8\pi^2 ieV\theta P^{(s)}}{\omega} \frac{1}{\frac{\gamma_0}{|\gamma_\mathbf{g}|}\left(-\chi_0 - \frac{2}{\omega}\frac{\gamma_0}{\gamma_\mathbf{g}}\lambda_\mathbf{g} + \beta\frac{\gamma_0}{\gamma_\mathbf{g}}\right)} \delta(\lambda_\mathbf{g}^* - \lambda_\mathbf{g}), \tag{9}$$

where $\lambda_\mathbf{g}^* = \frac{\omega\beta}{2} + \frac{\gamma_\mathbf{g}}{\gamma_0}\lambda_0^*$, $\lambda_0^* = \omega\left(\frac{\gamma^{-2}+\theta^2-\chi_0}{2}\right)$, $\delta(\lambda_0^* - \lambda_0) = \frac{|\gamma_\mathbf{g}|}{\gamma_0}\delta\left(\lambda_\mathbf{g}^* - \lambda_\mathbf{g}\right)$.

The incident and diffracted field inside the crystal as

$$E_0^{(s)\mathrm{cr}} = \frac{8\pi^2 ieV\theta P^{(s)}}{\omega} \frac{(-\omega^2\beta - 2\omega\frac{\gamma_\mathbf{g}}{\gamma_0}\lambda_0)\delta(\lambda_0 - \lambda_0^*)}{4\frac{\gamma_\mathbf{g}}{\gamma_0}(\lambda_0 - \lambda_0^{(1)})(\lambda_0 - \lambda_0^{(2)})} + E^{(s)^{(1)}}\delta\left(\lambda_0 - \lambda_0^{(1)}\right) + E^{(s)^{(2)}}\delta\left(\lambda_0 - \lambda_0^{(2)}\right) \tag{10a}$$

$$E_\mathbf{g}^{(s)\mathrm{cr}} = \frac{8\pi^2 ieV\theta P^{(s)}}{\omega} \frac{\omega^2\chi_\mathbf{g}C^{(s,\tau)}}{4\frac{\gamma_0^2}{\gamma_\mathbf{g}^2}(\lambda_\mathbf{g} - \lambda_\mathbf{g}^{(1)})(\lambda_\mathbf{g} - \lambda_\mathbf{g}^{(2)})}\delta(\lambda_\mathbf{g}^* - \lambda_\mathbf{g}) + E^{(s)^{(1)}}\delta\left(\lambda_\mathbf{g} - \lambda_\mathbf{g}^{(1)}\right) + E^{(s)^{(2)}}\delta\left(\lambda_\mathbf{g} - \lambda_\mathbf{g}^{(2)}\right), \tag{10b}$$

where $E^{(s)^{(1)}}$ and $E^{(s)^{(2)}}$ are the free fields, corresponding to the two solutions (8) of dispersion equation (6), and the fields in the vacuum behind the crystal as

$$E_0^{(s)\mathrm{vac\,II}} = \frac{8\pi^2 ieV\theta P^{(s)}}{\omega} \frac{1}{-\chi_0 - \frac{2\lambda_0}{\omega}}\delta(\lambda_0 - \lambda_0^*) + E_0^{(s)\mathrm{Rad}}\delta\left(\lambda_0 + \frac{\omega\chi_0}{2}\right), \tag{10c}$$

$$E_\mathbf{g}^{(s)\mathrm{vac}} = E_\mathbf{g}^{(s)\mathrm{Rad}}\delta\left(\lambda_\mathbf{g} + \frac{\omega\chi_0}{2}\right), \tag{10d}$$

where $E_0^{(s)\mathrm{Rad}}$, $E_\mathbf{g}^{(s)\mathrm{Rad}}$ is the coherent radiation amplitude in the electron velocity and Bragg directions appropriately.

3. – Spectral-angular density of the radiation in Bragg direction

For definition of amplitudes $E_0^{(s)\mathrm{Rad}}$ and $E_\mathbf{g}^{(s)\mathrm{Rad}}$ the ordinary boundary conditions on the inlet and outlet surfaces of the crystal plate are used and by substituting derived formulae for $E_\mathbf{g}^{(s)\mathrm{Rad}}$ to the well-known [22] expression for spectral-angular density of X-radiation

$$\omega\frac{\mathrm{d}^2N}{\mathrm{d}\omega\mathrm{d}\Omega} = \omega^2(2\pi)^{-6}\sum_{s=1}^{2}\left|E_\mathbf{g}^{(s)\mathrm{cr}}\right|^2, \tag{11}$$

the expression for PXR spectral-angular distribution is obtained:

$$\omega\frac{\mathrm{d}^2N^{(s)}_{\mathrm{PXR}}}{\mathrm{d}\omega\mathrm{d}\Omega}=\frac{e^2}{\pi^2}\frac{{P^{(s)}}^2\theta^2}{(\theta^2+\gamma^{-2}-\chi'_0)^2}R^{(s)}_{\mathrm{PXR}}, \tag{12}$$

$$R^{(s)}_{\mathrm{PXR}}=R^{(1)^{(s)}}_{\mathrm{PXR}}+R^{(2)^{(s)}}_{\mathrm{PXR}}+R^{(\mathrm{INT})^{(s)}}_{\mathrm{PXR}}$$

$$R^{(1)^{(s)}}_{\mathrm{PXR}}=\frac{\left(\xi^{(s)}-\sqrt{\xi^{(s)^2}-\varepsilon}\right)^2}{\Delta(\omega,\varepsilon)}\frac{\sin^2\left(b^{(s)}\left(\Delta^-(\omega,\varepsilon)-\sigma^{(s)}\right)/2\right)}{\left(\Delta^-(\omega,\varepsilon)-\sigma^{(s)}\right)^2}, \tag{13}$$

$$R^{(2)^{(s)}}_{\mathrm{PXR}}=\frac{\left(\xi^{(s)}+\sqrt{\xi^{(s)^2}-\varepsilon}\right)^2}{\Delta(\omega,\varepsilon)}\frac{\sin^2\left(b^{(s)}\left(\Delta^+(\omega,\varepsilon)-\sigma^{(s)}\right)/2\right)}{\left(\Delta^+(\omega,\varepsilon)-\sigma^{(s)}\right)^2}, \tag{14}$$

$$R^{(\mathrm{INT})^{(s)}}_{\mathrm{PXR}}= \tag{15}$$

$$\frac{\varepsilon\cos\left((b^{(s)}\sqrt{\xi^{(s)^2}-\varepsilon})/\varepsilon\right)\left(\cos\left(b^{(s)}\left(\xi^{(s)}/\varepsilon-\sigma^{(s)}\right)\right)-\cos\left((b^{(s)}\sqrt{\xi^{(s)^2}-\varepsilon})/\varepsilon\right)\right)}{\Delta(\omega,\varepsilon)\left(\left(\xi^{(s)}/\varepsilon-\sigma^{(s)}\right)^2+(\varepsilon-\xi^{(s)^2})/\varepsilon^2\right)},$$

where

$$\xi^{(s)}=\xi^{(s)}(\omega)=\eta^{(s)}(\omega)+\frac{(1+\varepsilon)}{2\nu^{(s)}}, \tag{16}$$

$$\eta^{(s)}(\omega)=\frac{2\sin^2\theta_B}{V^2|\chi'_{\mathbf{g}}C^{(s)}|}\left(\frac{\omega_B(1+\theta\cos\varphi\cot\theta_B)}{\omega}-1\right),$$

$$\varepsilon=\frac{|\gamma_{\mathbf{g}}|}{\gamma_0}, \qquad \sigma^{(s)}=\frac{1}{|\chi'_{\mathbf{g}}C^{(s)}|}\left(\theta^2+\gamma^{-2}-\chi'_0\right), \qquad b^{(s)}=\frac{\omega|\chi'_{\mathbf{g}}|C^{(s)}}{2}\cdot\frac{L}{\gamma_0},$$

$$\Delta^+(\omega,\varepsilon)=\frac{\xi^{(s)}+\sqrt{\xi^{(s)^2}-\varepsilon}}{\varepsilon},$$

$$\Delta^-(\omega,\varepsilon)=\frac{\xi^{(s)}-\sqrt{\xi^{(s)^2}-\varepsilon}}{\varepsilon}, \quad \Delta(\omega,\varepsilon)={\xi^{(s)}}^2-\varepsilon+\varepsilon\sin^2\left(\frac{b^{(s)}\sqrt{\xi^{(s)^2}-\varepsilon}}{\varepsilon}\right).$$

Here the PXR spectrum is represented in the form of the sum of two spectra, $R^{(1)^{(s)}}_{\mathrm{PXR}}$ and $R^{(2)^{(s)}}_{\mathrm{PXR}}$, corresponding to the two branches of dispersion equation and the summand $R^{(\mathrm{INT})^{(s)}}_{\mathrm{PXR}}$ is the result of their interference.

The function $R^{(s)}_{\mathrm{PXR}}$ describes the PXR spectrum. Parameter $b^{(s)}$ numerically equals half of the ratio of the relativistic electron path length $L/(2\gamma_0)$ and the length of X-radiation extinction $1/\omega|\chi'_{\mathbf{g}}C^{(s)}|$ in the crystal. The asymmetry parameter ε can be represented as $\varepsilon=\sin(\theta_B-\delta)/\sin(\theta_B+\delta)$, where θ_B is the angle between the electron velocity and the diffracting atomic plane. Hence we can see that parameter ε increases when the angle of electron incidence $(\theta_B+\delta)$ decreases and vice versa (see fig. 2).

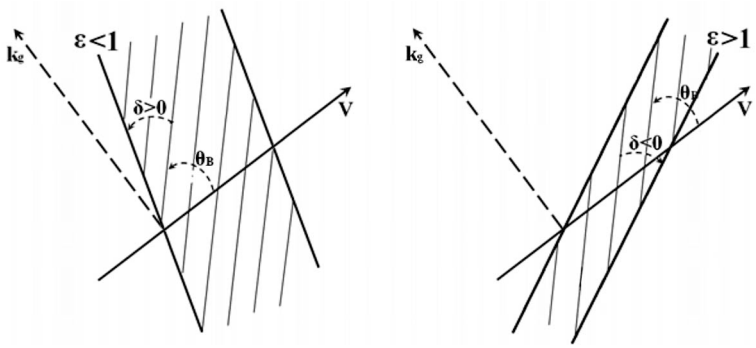

Fig. 2. – Circuitry of asymmetric ($\varepsilon > 1$, $\varepsilon < 1$) reflection of the radiation from single crystal plate. The case of $\varepsilon = 1$ corresponds to the symmetric reflection ($\delta = 0$).

4. – Spectral-angular density of the radiation in the direction of incident electron velocity

Substituting derived formulae for $E_0^{(s)\mathrm{Rad}}$ to (11) we will obtain the expressions describing the FPXR spectral-angular density:

$$\omega \frac{\mathrm{d}^2 N_{\mathrm{FPXR}}^{(s)}}{\mathrm{d}\omega \mathrm{d}\Omega} = \frac{e^2}{\pi^2} \frac{{P^{(s)}}^2 \theta^2}{(\theta^2 + \gamma^{-2} - \chi_0')^2} R_{\mathrm{FPXR}}^{(s)}, \tag{17}$$

$$R_{\mathrm{FPXR}}^{(s)} = R_{\mathrm{FPXR}}^{(1)^{(s)}} + R_{\mathrm{FPXR}}^{(2)^{(s)}} + R_{\mathrm{FPXR}}^{(\mathrm{INT})^{(s)}},$$

$$R_{\mathrm{FPXR}}^{(1)^{(s)}} = \frac{1}{\Delta(\omega,\varepsilon)} \frac{\sin^2\left(b^{(s)}\left(\Delta^-(\omega,\varepsilon) - \sigma^{(s)}\right)/2\right)}{\left(\Delta^-(\omega,\varepsilon) - \sigma^{(s)}\right)^2}, \tag{18}$$

$$R_{\mathrm{FPXR}}^{(2)^{(s)}} = \frac{1}{\Delta(\omega,\varepsilon)} \frac{\sin^2\left(b^{(s)}\left(\Delta^+(\omega,\varepsilon) - \sigma^{(s)}\right)/2\right)}{\left(\Delta^+(\omega,\varepsilon) - \sigma^{(s)}\right)^2}, \tag{19}$$

$$R_{\mathrm{FPXR}}^{(\mathrm{INT})^{(s)}} = \tag{20}$$

$$\frac{\cos\left((b^{(s)}\sqrt{\xi^{(s)^2} - \varepsilon})/\varepsilon\right)\left(\cos\left(b^{(s)}\left(\xi^{(s)}/\varepsilon - \sigma^{(s)}\right)\right) - \cos\left((b^{(s)}\sqrt{\xi^{(s)^2} - \varepsilon})/\varepsilon\right)\right)}{\Delta(\omega,\varepsilon)\left(\left(\xi^{(s)}/\varepsilon - \sigma^{(s)}\right)^2 + (\varepsilon - \xi^{(s)^2})/\varepsilon^2\right)}.$$

5. – Ratio of the PXR and FPXR yields

The contributions of the first (13), (18) and the second (14), (19) branches of PXR and FPXR spectra will be considerable under the conditions

$$\Delta^-(\omega,\varepsilon) - \sigma^{(s)} = 0, \tag{21}$$

$$\Delta^+(\omega,\varepsilon) - \sigma^{(s)} = 0. \tag{22}$$

The solution of eq. (21) or (22) defines the frequency in whose vicinity the PXR spectrum is concentrated at a certain observation angle. It follows from eqs. (21), (22) that the

maxima of the and FPXR spectra is situated out of the frequency region of the radiation total reflection (extinctions):

$$\xi^{(s)}(\omega) = \sqrt{\varepsilon} + \frac{\left(\sigma^{(s)}\sqrt{\varepsilon} - 1\right)^2}{2\sigma^{(s)}} > \sqrt{\varepsilon}, \tag{23}$$

therefore formulas (13)-(15) and (17)-(20) correctly describe the PXR and FPXR spectra for a thin crystal.

Equation (21) is soluble only under the condition

$$\varepsilon < \frac{1}{\sigma^{(s)^2}} \quad \text{or} \quad \varepsilon < \frac{\nu^{(s)^2}}{\left(P(\theta,\gamma)+1\right)^2}\,. \tag{24}$$

where $P(\theta,\gamma) = \theta^2/|\chi_0'| + \gamma^{-2}/|\chi_0'|$.

One can prove that eq. (22) has a solution under the condition

$$\varepsilon > \frac{1}{\sigma^{(s)^2}} \quad \text{or} \quad \varepsilon > \frac{\nu^{(s)^2}}{\left(P(\theta,\gamma)+1\right)^2}. \tag{25}$$

When the strong reflection of X-ray waves from the atomic planes takes place, the parameter $\nu^{(s)} = \frac{|\chi_{\mathbf{g}}' C^{(s)}|}{|\chi_0'|}$ is close to 1, in the case of weak reflection the parameter $\nu^{(s)} \approx 0$. Since $\nu^{(s)} < 1$, than inequality (25) is satisfiable in the case when $\varepsilon \geq \nu^{(s)^2}$ and it means that only eq. (22) is soluble and the contribution to PXR and FPXR gives only the second branch of dispersion equation solution. In the case when $\varepsilon < \nu^{(s)^2}$ both inequalities (24) and (25) can be satisfiable as a function of the observation angle θ and the relativistic electron energy γ. It means that for this case both branches of the excited X-ray wave can give the contribution to PXR and FPXR yields.

Let us consider the case when the inequality (25) is complete. In this case the second branches of PXR and FPXR give the main contribution to radiation yield and the spectra ratio has the form which follows from (14) and (19):

$$R_{\mathrm{PXR}}^{(2)^{(s)}} / R_{\mathrm{FPXR}}^{(2)^{(s)}} = \left(\xi^{(s)} + \sqrt{\xi^{(s)^2} - \varepsilon}\right)^2. \tag{26}$$

It follows from expression (26) with taking into account (23) that in case when $\varepsilon > 1$ or $\varepsilon \approx 1$, the PXR yield exceeds considerably the FPXR yield $R_{\mathrm{PXR}}^{(2)^{(s)}} \gg R_{\mathrm{FPXR}}^{(2)^{(s)}}$. To demonstrate this fact the curves plotted by formulas (14) and (19) are presented in fig. 3 for the parameters pointed in the picture. As was expected, the PXR yield materially exceeds the FPXR yield.

At the increase of the parameter ε, *i.e.* increase of the angle of particle incidence to the target surface $\delta + \theta_B$ (see in fig. 2), the intensity of FPXR (at a small angle to particle velocity) can considerably exceed the intensity of PXR in Bragg scattering direction $R_{\mathrm{PXR}}^{(2)^{(s)}} \ll R_{\mathrm{FPXR}}^{(2)^{(s)}}$, which is demonstrated by the curves in fig. 4. In the considered case the PXR photon will move from the plate at a small angle to its surface (see in fig. 2).

When we use eq. (22), whose solution is the frequency in the vicinity of which the PXR photon spectrum is concentrated and the amplitude maximum is situated, we will

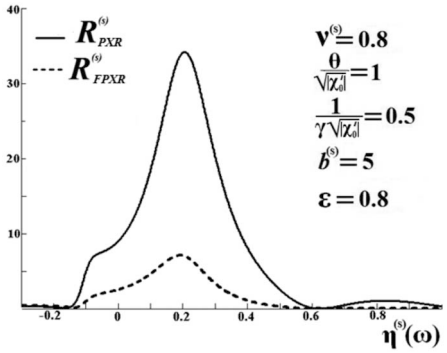

Fig. 3.

write expression (26) as

$$R^{(2)^{(s)}}_{\mathrm{PXR}}/R^{(2)^{(s)}}_{\mathrm{FPXR}} = (\varepsilon^2/\nu^{(s)^2})\left(\theta^2/|\chi'_0| + \gamma^{-2}/|\chi'_0| + 1\right)^2. \tag{27}$$

This ratio allows us to estimate the relative contributions of the radiations as a function of the observation angle θ, the radiating particle energy defined by the Lorentz factor γ, and the parameter $\nu^{(s)}$.

It results from (37) that at observation angle decrease the FPXR yield more and more exceeds the PXR yield for low values of the asymmetry parameter ε.

We can obtain this ratio for the PXR angle density maximum ($\theta = \sqrt{\gamma^{-2} + |\chi'_0|}$) in the following form:

$$R^{(2)^{(s)}}_{\mathrm{PXR}}/R^{(2)^{(s)}}_{\mathrm{FPXR}} = (2\varepsilon^2/\nu^{(s)^2})\left(\gamma^{-2}/|\chi'_0| + 1\right)^2. \tag{28}$$

As the value of parameter $\nu^{(s)}$ is always less than 1, it follows from expression (38) that for $\gamma^2|\chi'_0| \ll 1$ the PXR yield will practically always exceed the FPXR yield. Otherwise, for $\gamma^2|\chi'_0| \geq 1$ this ratio can become close or less than 1 for a small value of the asymmetry parameter ε. In this case the feature of PXR and FPXR contribution to the total

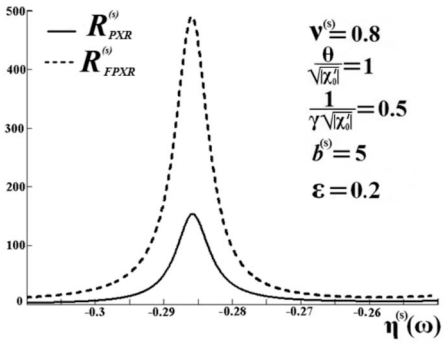

Fig. 4.

radiation yields considerably depends on the asymmetry of relativistic particle Coulomb field reflection (parameter ε).

Let us consider the case when inequality (24) is completed. In this case both branches give the contribution to the radiation and their interference can be considerable. For this case the ratio of the first branch of the PXR and FPXR waves following from (13) and (18) has the following view:

$$R_{\mathrm{PXR}}^{(1)^{(s)}} / R_{\mathrm{FPXR}}^{(1)^{(s)}} = \left(\xi^{(s)} - \sqrt{\xi^{(s)^2} - \varepsilon}\right)^2 . \tag{29}$$

As it follows from comparison of (26) and (29) in the last case the FPXR yield much more exceeds the PXR yield for small values of ε. So under decrease of ε it is the first branch of excited X-ray waves which makes the main contribution to the radiation and it leads to the increase of FPXR yield.

6. – Conclusion

Based on two-wave approximation of the dynamic scattering theory analytical expressions for the spectral-angular distribution of FPXR and PXR in Bragg scattering direction are derived in the general case of asymmetric reflection for Bragg scattering geometry.

The analyses of the obtained expressions have shown that at a fixed angle between relativistic electron velocity and the system of diffracted atomic planes θ_B and length of electron path in the crystal plate $2b^{(s)}$ the ratio of the PXR and FPXR yields depends significantly on the angle between reflecting atomic planes and the inlet surface of the plate, *i.e.* on reflection asymmetry. The decrease of the asymmetry parameter $\varepsilon = \sin(\delta - \theta_B)/\sin(\delta + \theta_B)$ (increase of the angle $\delta + \theta_B$ of the electron incidence on the crystal plate) results in the decrease of PXR spectral-angular density and the increase of FPXR density which can exceed the density of PXR when the parameter ε value becomes small enough.

REFERENCES

[1] Ter-Mikaelian M., *High-Energy Electromagnetic Process in Condensed Media* (Wiley, New York) 1972.
[2] Garibian G. and Yang C., *J. Exp. Theor. Phys.*, **61** (1971) 930.
[3] Baryshevsky V. and Feranchuk I., *J. Exp. Theor. Phys.*, **61** (1971) 944.
[4] Garibian G. and Yang C., *J. Exp. Theor. Phys.*, **63** (1972) 1198.
[5] Baryshevsky V. and Feranchuk I., *Phys. Lett. A*, **57** (1976) 183.
[6] Baryshevsky V. and Feranchuk I., *J. Phys. (Paris)*, **44** (1983) 913.
[7] Yuan Luke C., Alley P., Bamberger A. *et al.*, *Nucl. Instrum. Methods Phys. Res. A*, **234** (1985) 426.
[8] Kalinin B., Naumenko G., Padalko D. *et al.*, *Nucl. Instrum. Methods Phys. Res. B*, **173** (2001) 253.
[9] Kube G., Ay C., Backe H., Clawiter N. *et al.*, *Abstracts V International Symposium on Radiation from Relativistic Electrons in Periodic Structures, Lake Aya, Altai Mountains, Russia, 10-14 September 2001.*
[10] Backe H., Clawiter N. *et al.*, *Proceedings of the International Symposium on Channeling –Bent Crystals – Radiation Processes, Frankfurt am Main, Germany, EP Systema Bt., Debrecen* (2003), p. 41.

[11] Aleinik A., Baldin A., Bogomasova E., Vnukov I. *et al.*, *J. Exp. Theor. Phys. Lett.*, **80** (2004) 447.
[12] Imanishi N., Nasonov N. and Yajima K., *Nucl. Instrum. Methods Phys. Res. B*, **173** (2001) 227.
[13] Kubankin A., Nasonov N., Sergienko V. and Vnukov I., *Nucl. Instrum. Methods Phys. Res. B*, **201** (2003) 97.
[14] Nasonov N. and Noskov A., *Nucl. Instrum. Methods Phys. Res. B*, **201** (2003) 67.
[15] Kubankin A., Nasonov N. and Noskov A., *Proceedings of 7 International Russian-Japanese Symposium on Interaction of fast charged particles with solids, Nov. 24-30, Kyoto, Japan* (2002), pp. 217-225.
[16] Blazhevich S. and Noskov A., *Nucl. Instrum. Methods Phys. Res. B*, **252** (2006) 69.
[17] Blazhevich S. and Noskov A., *Nucl. Instrum. Methods Phys. Res. B*, **266** (2008) 3770.
[18] Blazhevich S. and Noskov A., *Nucl. Instrum. Methods Phys. Res. B*, **266** (2008) 3777.
[19] Blazhevich S. and Noskov A., *Russ. Phys. J.*, **50** (2006) 574.
[20] Blazhevich S. and Noskov A., *J. Phys.: Conf. Ser.*, **236** (2010) 012013.
[21] Pinsker Z., *Dynamic Scattering of X-rays in Crystals* (Springer, Berlin) 1984.
[22] Bazylev V. and Zhevago N., *Emission From Fast Particles Moving in a Medium and External Fields* (Nauka, Moscow) 1987.